# A First Comparison of the responses of a $^4$He-based fast-neutron detector and a NE-213 liquid-scintillator reference detector

R. Jebali[a,1], J. Scherzinger[b,d], J.R.M. Annand[c], R. Chandra[a], G. Davatz[a], K.G. Fissum[b,d,*], H. Friederich[a], U. Gendotti[a], R. Hall-Wilton[d,f], E. Håkansson[b], K. Kanaki[d], M. Lundin[e], D. Murer[a], B. Nilsson[d,e], A. Rosborg[e], H. Svensson[e,g]

[a] *Arktis Radiation Detectors Limited, 8045 Zürich, Switzerland*
[b] *Division of Nuclear Physics, Lund University, SE-221 00 Lund, Sweden*
[c] *University of Glasgow, Glasgow G12 8QQ, Scotland, UK*
[d] *Detector Group, European Spallation Source ESS AB, SE-221 00 Lund, Sweden*
[e] *MAX IV Laboratory, Lund University, SE-221 00 Lund, Sweden*
[f] *Mid-Sweden University, SE-851 70 Sundsvall, Sweden*
[g] *Sweflo Engineering, SE-275 63 Blentarp, Sweden*

**Abstract**

A first comparison has been made between the pulse-shape discrimination characteristics of a novel $^4$He-based pressurized scintillation detector and a NE-213 liquid-scintillator reference detector using an Am/Be mixed-field neutron and gamma-ray source and a high-resolution scintillation-pulse digitizer. In particular, the capabilities of the two fast neutron detectors to discriminate between neutrons and gamma-rays were investigated. The NE-213 liquid-scintillator reference cell produced a wide range of scintillation-light yields in response to the gamma-ray field of the source. In stark contrast, due to the size and pressure of the $^4$He gas volume, the $^4$He-based detector registered a maximum scintillation-light yield of 750 keV$_{ee}$ to the same gamma-ray field. Pulse-shape discrimination for particles with scintillation-light yields of more than 750 keV$_{ee}$ was excellent in the case of the $^4$He-based detector. Above 750 keV$_{ee}$ its signal was unambiguously neutron, enabling particle identification based entirely upon the amount

*Corresponding author. Telephone: +46 46 222 9677; Fax: +46 46 222 4709
*Email address:* kevin.fissum@nuclear.lu.se (K.G. Fissum)
[1] present address: University of Glasgow, Glasgow G12 8QQ, Scotland, UK

of scintillation light produced.

*Keywords:* $^4$He, NE-213, scintillation, gamma-rays, fast neutrons, digitizer, pulse-shape discrimination

## 1. Introduction

Fast neutrons are important both as probes of matter and as diagnostic tools [1–14]. In the case that information about the energy and emission time of a neutron is available, conclusions about its origin can be drawn. The timing precision required to obtain this information may only be provided by neutron detectors that are fast, providing signals with short risetimes. Today, organic liquid scintillators are the detectors-of-choice for fast neutrons. Drawbacks associated with these scintillators are their toxicity, reactive nature, and sensitivity to a broad range of gamma-ray energies.

Scintillators are substances which emit light when subjected to ionizing radiation. The characteristic time constant associated with the light emitted is a function of the properties of the scintillator in question. Certain scintillators respond to different types of ionizing radiation differently; that is, the time constant of the emitted light is different depending upon the density of ionization produced by the incident radiation. Normally, there are several components with different time constants. The relative intensity of these components affects the effective integrated time constant. By carefully analyzing the behavior of the scintillation light as a function of time, one can determine the incident particle type. This procedure is called pulse-shape discrimination (PSD). PSD is often used to distinguish between different types of uncharged particles, namely gamma-rays and neutrons. In scintillators with good PSD properties, incident gamma-rays interact primarily with the atomic electrons of the scintillator, producing close to minimum-ionizing electrons which give a fast (decay times of some 10s of ns) flash of light. On the other hand, incident neutrons interact primarily with the hydrogen in liquid scintillators and $^4$He nuclei in noble-gas scintillators via scattering, transferring some of their energy. For hydrogen, this

energy transfer can be 100%, while for $^4$He, the energy transfer is at best 64%. The resulting flashes of light arising from the much denser ionization produced by the relatively large energy loss of the recoiling protons and alpha particles have longer decay times (100s to 1000s of ns). PSD and thus incident particle identification may be performed by recording the time dependence of the scintillation pulse form and comparing the fast and slow components.

## 2. $^4$He as a scintillation medium for fast neutron detection

The development of both liquid and gaseous $^4$He based scintillators for fast-neutron detection has been reported [6, 8, 12, 14, 15]. $^4$He, like most noble gases, is a good scintillator. It has an ultra-violet light yield comparable to the intrinsic non-Tl doped light yield of NaI crystals [16–19]. Neutron interactions lead to $^4$He recoils, where energy is deposited very locally within the gas. Gamma-ray interactions lead to recoiling electrons, which deposit only tens of keV per centimeter of trajectory. This difference in deposition density and therefore ionization density is believed to ultimately enable the PSD capability. PSD properties may be degraded significantly if the geometry and size of the detector results in a smearing of the transit times of scintillation photons comparible to the scintillation decay times. Good PSD also requires good scintillation efficiency; that is, a sufficient number of scintillation photons to define the time dependence of the pulse accurately, and low noise in the pulse-processing electronics.

With only two electrons per atom, $^4$He has a very low charge density, thereby significantly limiting its sensitivity to gamma-rays. This is useful for fast-neutron detection, where insufficient gamma-ray rejection is often the factor which constrains the desired performance. The following physical effects contribute positively to the gamma-ray rejection performance of pressurized $^4$He gas:

1. *Low gamma-ray interaction probability.* Due to the low electron density of $^4$He, gamma-ray interaction probabilities are two orders of magnitude

lower than neutron interaction probabilities.

2. *Low energy deposition.* Depending on the chosen geometry (i.e. a tube with radius of a few cm), the amount of energy the gamma-rays can deposit in the detector volume is limited. This is because the corresponding Compton or pair electrons cannot transfer much energy to the gas before striking a detector wall.
3. *Similar scintillation-light yield for gamma-rays and neutrons.* The scintillation light production in organic liquid scintillators is highly velocity dependent. Thus, for the same amount of deposited energy, gamma-ray interactions produce more scintillation light than neutron interactions. In contrast, the scintillation-light yield for gamma-rays and neutrons is similar in noble-gas scintillators [17] such as $^4$He. $^4$He is commonly called a linear scintillator.
4. *PSD.* 1–3 above together with the fast and slow components of the $^4$He scintillation signals lead to excellent PSD and thus excellent separation of neutrons and gamma-rays.

The purpose of this project was to compare the neutron/gamma discrimination obtained using the Arktis $^4$He-based neutron-diagnostic tool (NDT) to that obtained using a reference liquid-scintillator cell filled with the organic liquid scintillator NE-213 [20].

## 3. Apparatus

### *3.1. Am/Be source*

The detector characterizations reported on in this paper were carried out using a nominal 18.5 GBq $^{241}$Am/$^9$Be (Am/Be) source [21] which emitted $(1.106\pm0.015) \times 10^6$ neutrons per second nearly isotropically [22]. The source is a mixture of americium oxide and beryllium metal contained in an X.3 capsule, which is a stainless-steel cylinder 31 mm (height) × 22.4 mm (diameter) [23]. $^{241}$Am has a half-life of 432.2 years and decays via alpha emission (5 discrete energies with an average value of about 5.5 MeV) to $^{237}$Np. The dominant energy

of the gamma-rays associated with the decay of the intermediate excited states in $^{237}$Np is ∼60 keV. A 3 mm thick Pb sheet was used to complement the stainless steel X.3 capsule to attenuate these 60 keV gamma-rays. The half-value layer for Pb for 60 keV gamma-rays is 0.12 mm, while for 1 MeV gamma-rays, it is 8 mm. Neutrons are produced when the emitted alpha particles undergo a nuclear reaction with $^{9}$Be resulting in $^{12}$C and a free neutron. The resulting neutron distribution has a maximum energy of about 11 MeV [24], while approximately 25% of the neutrons have an energy of less than 1 MeV [25]. The de-excitation of the $^{12}$C results in a 4.44 MeV gamma-ray about 55% of the time [25–27]. This gamma-ray is too energetic to be absorbed by the stainless steel of the X.3 capsule. Thus the radiation field from the Am/Be is a combination of high-energy gamma-rays and fast neutrons. Both the gamma-ray and fast-neutron dose rates at a distance of 1 m from the source in the unshielded X.3 capsule were measured using a Thermo Scientific Corporation FHT 752 dosimetric neutron detector [28]. They were both determined to be 11 $\mu$Sv/hr for a total unshielded dose rate of 22 $\mu$Sv/hr, in exact agreement with the data sheet from the supplier.

### *3.2. Arktis pressurized $^{4}$He gas Neutron Diagnostic Tool (NDT)*

The version of the Arktis pressurized gas $^{4}$He fast NDT used for these measurements is shown in Fig. 1. It was of cylindrical geometry with an outer diameter of 5.08 cm (2") and a 19.5 cm active length. The detector walls were made of stainless steel. The interior surface of the stainless-steel cylinder was coated with a PTFE-based diffuse reflector [29] which was itself coated with an organic phosphor that converted the wavelength of the scintillation light from 80 nm to 430 nm. As $^{4}$He is transparent to its own light, almost no signal loss due to reabsorption occurs [30]. The predominant mechanism for signal loss was due to multiple reflections inside the detector. Optical windows capable of withstanding the 120 bar operating pressure were employed. The scintillation signals were read out at both ends of the active volume by Hamamatsu R580 [31] photomultiplier tubes (PMTs).

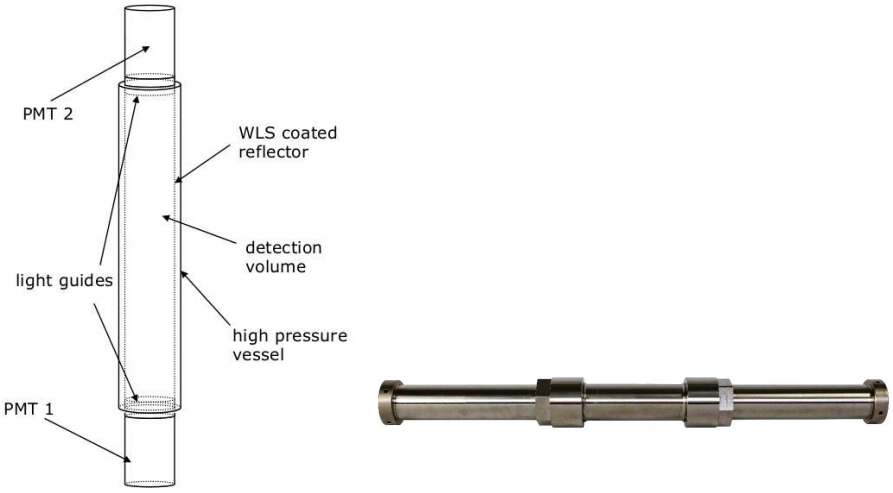


Figure 1: Schematic (left) and photograph (right) of the pressurized $^4$He gas fast-neutron detector. The outer diameter was 5.08 cm (2") and the active length was 19.5 cm.

### *3.3. NE-213 reference detector*

The NE-213 reference detector is shown in Fig. 2. The core of the NE-213 reference detector was a 3 mm thick cylindrical aluminum cell with an inner depth of 62 mm and an inner diameter of 94 mm. The inside of the cell was painted with EJ-520 [32] titanium dioxide reflective paint, which can withstand the xylene solvent of the liquid scintillator. The aluminum cell was sealed using a 5 mm thick borosilicate glass window [33] glued to the aluminum cell using the highly temperature and chemical resistant Araldite 2000+ [34]. The 2 penetrations into the cell which allowed for filling were sealed with M-8 threaded aluminum plugs with 20 mm diameter heads and 14 mm diameter Viton O-rings [35]. Nitrogen gas was bubbled through the NE-213 liquid scintillator for 24 hours prior to filling the cell. The assembled cell was then filled with the nitrogen-flushed NE-213 using a nitrogen gas transfer system.

After filling, the borosilicate glass window of the cell was coupled to a cylindrical PMMA [36] lightguide with a depth of 57 mm and a diameter of 72.5 mm. PMMA is an acrylic which transmits light down to 300 nm in wavelength [37].

Figure 2: The NE-213 reference detector. Top: a detail of the cylinder "cup". The screws on top allow for the filling or draining of the liquid cylinder. A borosilicate-glass window (light brown) serves as the optical boundary. See text for details. Bottom: The black cylinder to the right is the magnetically shielded 3 inch ET Enterprises 9821KB photomultiplier-tube assembly. The gray cylinder to the left is the "cup". (For interpretation of the references to color in this figure caption, the reader is referred to the web version of this article.)

The cylindrical surface of this lightguide was painted with water-soluble EJ-510 [38] reflective paint. The lightguide was then pressure-coupled via springs to a magnetically shielded 3 inch ET Enterprises 9821KB PMT assembly [39]. As our goal was to produce a stable detector which provided reproducible results, no optical-coupling grease was used.

### *3.4. Arktis WaveDREAM-B16 digitizer*

The analog signals from the NDT and NE-213 reference cell were fed directly to a WaveDREAM-B16 high-precision digitizer developed by Arktis Radiation Detectors [40] (see Fig. 3). After being converted to a digital signal, the data of interest were stored for analysis. The decision for storage was based on a 120 megasample per second (MSPS) signal that was continuously read out and fed into a field programmable gate array (FPGA). If the user-defined trigger condition was met (see below for the trigger conditions employed in this measurement), the FPGA read out the DRS4 switched capacitor array [41] contain-

ing the stored waveform at 1 gigasample per second (GSPS). Complete details are presented in Ref. [42]. In this manner, excellent time resolution (provided by the 1 GSPS sampling and nanosecond time stamping also between different detectors) was achieved at 10-bit resolution over the 3.5 $\mu$s duration of the stored event. The trigger conditions were user-configurable. In the case of the NDT, a trigger occurred only if the signals from both PMTs mounted on each end of the detector were above threshold. This threshold was 35 scintillation photons detected above the ambient baseline, and suppressed the dark-current count rate. An event was considered to be valid if the second PMT signal came less than 32 ns after the first, a criterion related to the speed of light, dimensions of the $^4$He gas volume, and response of the PMTs. This broad timing window in the digitizer was inherited from studies of a different system and was considered to be "safe" for the investigations of the much smaller NDT studied here. In the case of the NE-213 reference cell which had only one PMT, a trigger occurred if the analog signal coming from the PMT was above threshold. This threshold was 30 scintillation photons detected above the ambient baseline. The digitizer greatly facilitated the offline analysis of the data as it allowed for the Arktis NDT PMTs to be synchronized to better than 1 ns. It also allowed for offline variation in the detector thresholds and integration gates (see below), a clear advantage over standard discriminators and analog-to-digital converters.

## 4. Measurement

### *4.1. Setup*

The experiment setup is shown in Fig. 5. The Am/Be source in its transport/storage container was placed at the center of a 4-sided enclosure constructed from borated-wax boxes. In the so-called "park" position with the source locked in its transport container at the bottom of the borated-wax box enclosure, the total dose rate in the room was less than 0.4 $\mu$Sv/hr. When the source was lifted from its container and positioned within the 3 mm Pb

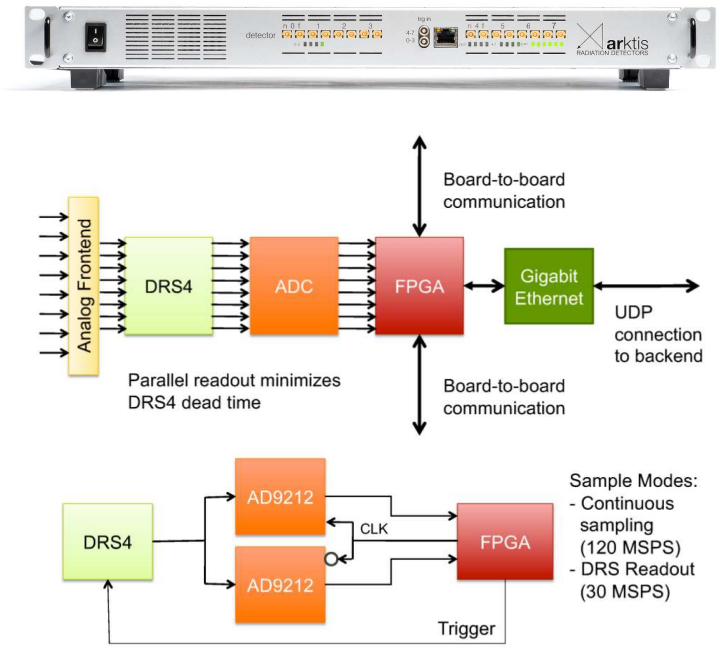


Figure 3: The top figure shows the WaveDREAM-B16. There are 16 input channels grouped in 2 clusters of 8. Once the selected signals are digitized, they are read out via Gigabit ethernet. Triggers can be applied externally or generated internally by the software. The middle figure is a schematic overview of the readout electronics. Signals are stored in the DRS4 switched-capacitor array and read out if user-defined trigger conditions are met. The bottom figure presents an overview of the software trigger. If the signal sampled at 120 MSPS meets the trigger condition, the FPGA reads out the DRS4 at 1 GSPS. See Ref. [42] for further details.

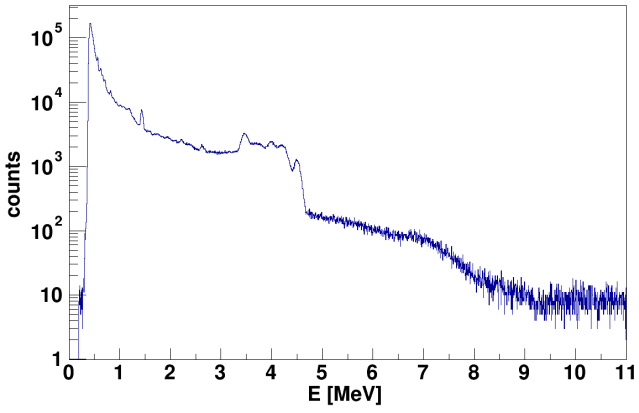


Figure 4: Energy distribution of gamma-rays at the approximate location of the NDT and NE-213 reference cell. The prominent structure between 3 and 5 MeV results from the 4.44 MeV gamma-ray.

thick sleeve, the gamma-ray dose rate on the outside of the 4-sided borated-wax enclosure was 1 $\mu$Sv/hr.

Square penetrations through 2 of the opposite walls of the enclosure allowed direct line-of-sight between the detectors being irradiated and the source. A HPGe gamma-ray detector was positioned in one of the apertures. The distance to the screened source was $\sim$1 m and line-of-sight was direct. It was used to measure the distribution of gamma-rays at the approximate location of the NDT and NE-213 reference cell. Fig. 4 presents this distribution, where the 4.44 MeV gamma-ray peak together with its Compton edge, first- and second-escape peaks, and their Compton edges are clearly seen between (from the right) 5 and 3 MeV. Between 1.0 MeV and the $\sim$400 keV detector threshold, the gamma-ray intensity increased by an order-of-magnitude.

At a distance of 0.54 m from the source, the square aperture for the NE-213 reference detector was $17 \times 17$ cm$^2$. The cell was placed at source height so that the face of the active volume (recall Fig. 2) was 70 cm from the center of the Am/Be source. The cylindrical symmetry axis of the detector pointed directly at the center of the source. It was operated at $-1700$ V. The analog signals

from the single PMT were fed into the digitizer. The digitized waveforms of the signals which triggered the acquisition were recorded on an event-by-event basis for offline processing. At the same distance from the source, the square aperture for the NDT was 25 $\times$ 25 cm$^2$. The NDT was also placed at source height. However, its cylindrical symmetry axis was perpendicular to the ray pointing to the center of the source. Both of the PMTs (one at each end of the detector volume) were operated at +1730 V. The analog signals from these PMTs were fed into the digitizer. Again, the digitized waveforms of the signals which triggered the acquisition were recorded on an event-by-event basis for offline processing.

A pulse-shape (PS) analysis of the analog signals coming from both detectors was performed using the "tail-to-total" method. Two integration gates were defined, a long gate (LG) and a short gate (SG). Both of the gates opened at the same time, 10 ns before the analog signal. The SG was used to integrate only the fast components of the analog signal, while the LG was used to integrate the entire (both fast and slow components) analog signal. The PS was determined from the difference between the scintillation-light yield in the LG and SG normalized to the scintillation-light yield in the LG: PS = (LG-SG)/LG. For the NDT PMT data, the SG was 100 ns (related to the decay constant of the fast-scintillation components of $^4$He) and the LG was 3500 ns (the maximum gate length the digitizer provided). For the NE-213 reference cell data, the SG was 25 ns and the LG was 150 ns. The Arktis NDT gate widths were optimized offline. This procedure was greatly facilitated by the digitizer.

### *4.2. Absolute energy calibration*

Energy-calibration measurements for the NE-213 reference cell were performed using $^{60}$Co, $^{137}$Cs, and the Pb-shielded Am/Be sources. $^{60}$Co emits gamma-rays with energies 1.17 MeV and 1.33 MeV. $^{137}$Cs emits a gamma-ray with an energy 0.66 MeV. The de-excitation gamma-ray from the first excited state of $^{12}$C has an energy of 4.44 MeV. The locations of the Compton edges from these gamma-rays were determined using the prescription of Knox and

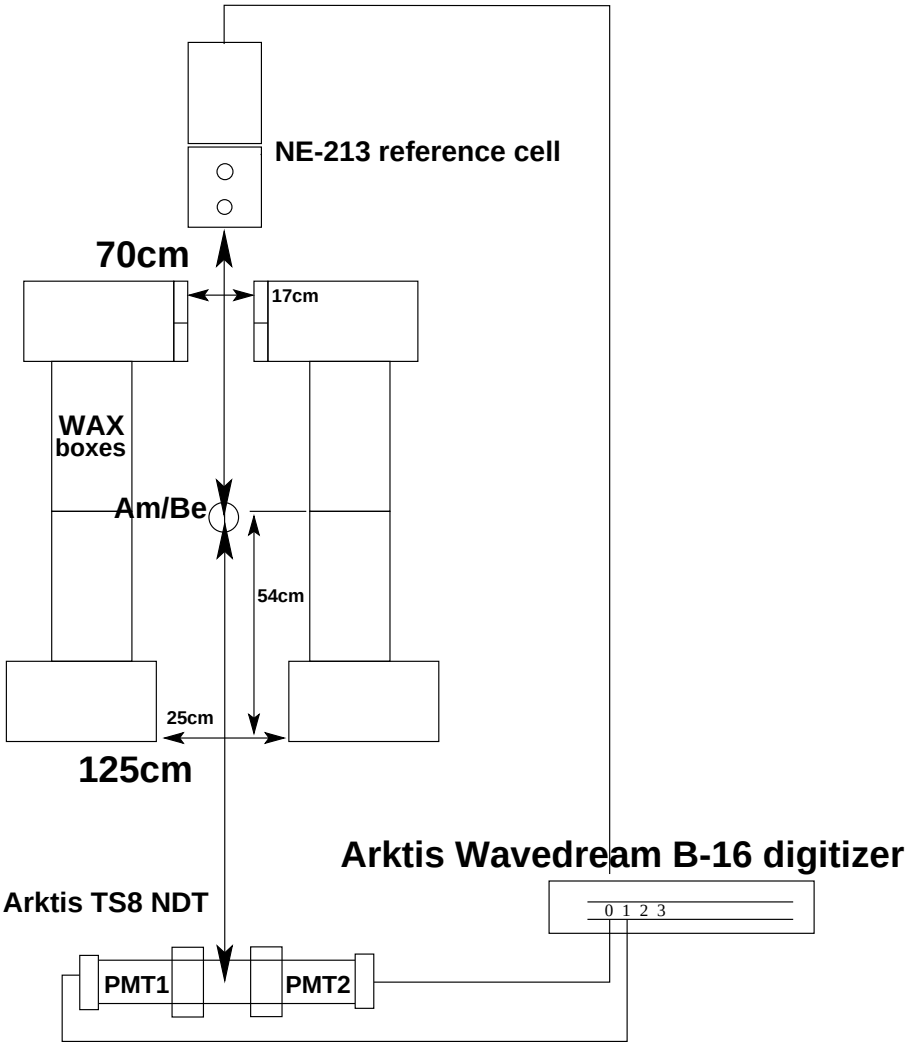


Figure 5: The experiment setup (not to scale). The Am/Be source was placed at the center of a borated-wax enclosure. Penetrations through two of the enclosure walls allowed for a direct line-of-sight between the source and the detectors. For measurements of the gamma-ray distribution at the apertures, the NE-213 reference cell was replaced with a stand-alone HPGe detector.

Miller [43].

For the NDT, Geant4 simulations [44, 45] reproduce the shape of the observed pulse-height distributions for neutrons and gamma-rays well. The $\alpha$ decay of trace amounts of $^{222}$Rn in the $^{4}$He gas of the NDT provides an energy signature similar to the neutron/$^{4}$He scattering process, and was used to calibrate the detector. Neutrons, which produce a recoiling $\alpha$ particle, were correlated directly to the 5.5, 6.0, and 7.7 MeV $\alpha$ lines in $^{222}$Rn [8]. Gamma-rays produce an electron via Compton scattering or an electron and positron via pair production. These interactions occur dominantly in the relatively high-Z walls of the NDT. Apart from very low energies, most electrons or positrons entering the $^{4}$He gas volume do not stop in the gas. On traversing the gas, they loose a fairly well-defined energy of around 150 keV. This produces a peak in the pulse-height distribution which can be used for cross calibration. The energy-loss distribution extends out to around 750 keV, which is more or less independent of the incident gamma-ray energies above 750 keV. These energy losses are of course dependent upon the size and pressure of the $^{4}$He gas volume. From this, we have established that the scintillation-light yield is the same for electrons and alpha particles, consistent with $^{4}$He being a linear scintillator. This contrasts with NE-213, where the scintillation-light yield depends strongly on the velocity and ionization density of the interacting particle.

## 5. Results

We stress that the data presented in this section came directly from the digitizer and were not optimized via offline software corrections in any way. Figure 6 shows a two-dimensional scatterplot comparison of the PSD achieved using the NE-213 reference cell and the $^{4}$He-based NDT obtained using the Pb-screened Am/Be source. Recall that the Pb-screened Am/Be source provided a continuous energy spectrum of neutrons up to 11 MeV and a of gamma-rays up to 4.44 MeV. The gamma-ray pulse-height response of the NE-213 reference cell extends to 4 MeV$_{ee}$ as shown in the upper panel. Below 500 keV$_{ee}$, significant

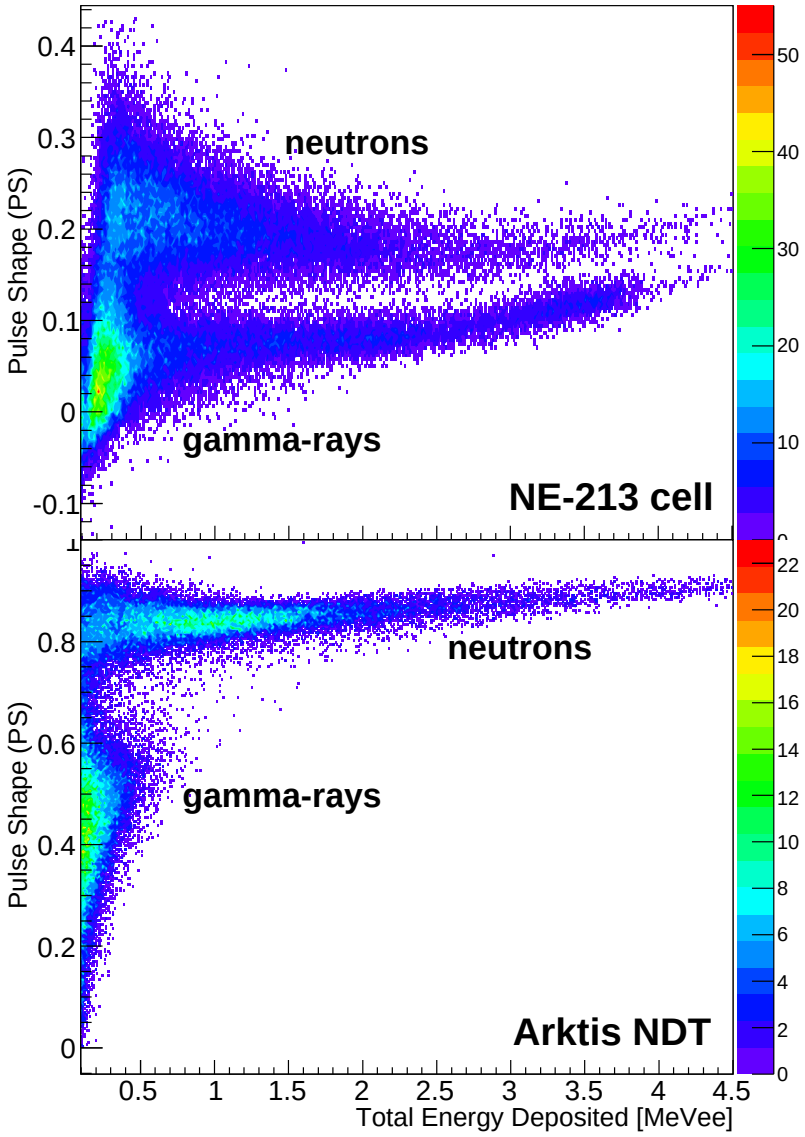


Figure 6: A comparison of the PSD achieved using the NE-213 reference cell (top panel) and the $^4$He-based NDT (bottom panel) with the Pb-screened Am/Be source. For each event, the signal pulse shape PS = (LG-SG)/LG has been plotted against the scintillation-light yield produced in the detector for the LG in MeV$_{ee}$. The distributions corresponding to neutrons and gamma-rays are labeled.

overlap between the neutron and gamma-ray pulse-height responses occurred. As shown in the lower panel and in stark contrast, the gamma-ray pulse-height response of the Arktis NDT extends only to 750 keV$_{ee}$, and clear separation between the neutron and gamma-ray pulse-height responses is evident down to 100 keV$_{ee}$.

The amount of scintillation light produced in the gaseous $^4$He is less than that produced in the liquid scintillator for both particle types. In absolute terms, the detection efficiency of the NE-213 reference cell will qualitatively be higher the Arktis NDT, both for neutrons and gamma-rays. Quantitative evaluation of these detection efficiencies and comparisons with Monte Carlo calculations will be addressed in a future publication. We note that the lower absolute detection efficiency of the Arktis NDT could be advantageous in very high intensity radiation fields. The complete lack of a gamma-ray band to higher energies in the bottom scatterplot is striking. Relative to the numbers of neutrons detected, the gamma-ray discrimination properties of the Arktis NDT are clearly superior. The digitizer clearly proved to be a very effective tool for optimizing the PSD.

One-dimensional projections of PS have been obtained from the two-dimensional distributions shown in Fig. 6 for five different pulse-height thresholds. The resulting PS distributions for the NE-213 detector (left column) and Arktis NDT (right column) integrated from these thresholds are shown in Fig. 7. In each of the panels, wherever possible, two separate Gaussian functions have been fitted to the data – one corresponding to gamma-rays (red) and one corresponding to neutrons (blue). A standard figure-of-merit (FOM) has been used to quantify the quality of the PSD as a function of deposited-energy cut. This FOM is given by the separation between the gamma-ray and neutron peaks divided by the sum of the FWHM of these peaks.

As can be seen in the NE-213 data (left column), the FOM improves from 0.75 to 1.5 as the requirement on the light yield increases from 0.25 to 3.0 MeV$_{ee}$. In comparison, the Arktis NDT FOM (right column) improves from 1.35 to 1.70 as the requirement on the light yield increases from 0.25 to 0.50

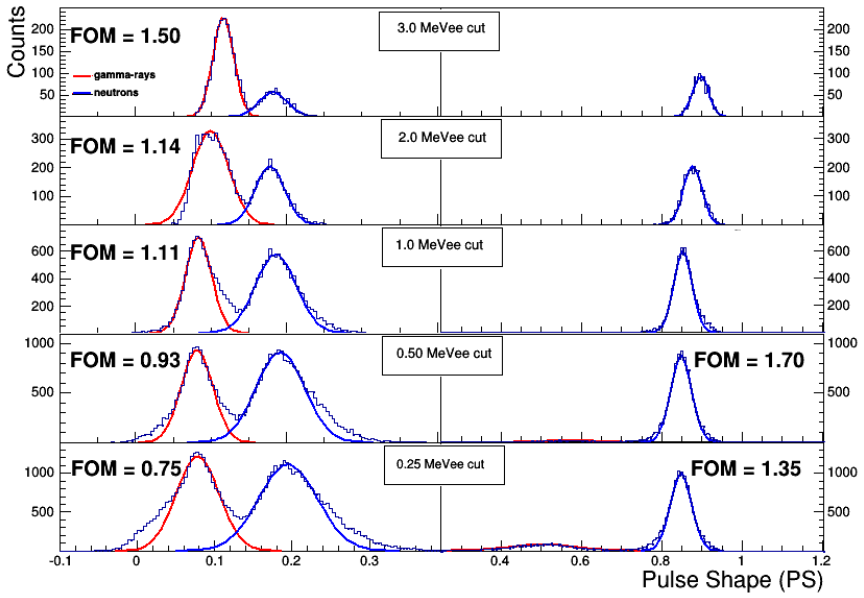


Figure 7: A first comparison of the PSD achieved using the NE-213 reference cell (left column) and the $^4$He-based NDT (right column) via a FOM using the Pb-screened Am/Be source and varying the requirements on the amount of energy deposited in the detectors. Gamma-rays with energies up to 4.44 MeV deposit no more than 750 keV$_{ee}$ in the Arktis NDT which greatly facilitates fast-neutron particle identification.

MeV$_{ee}$. Once the requirement on the amount of deposited energy exceeds 0.75 MeV$_{ee}$, the gamma-ray peak is no longer visible in the Arktis NDT, and the signal is unambiguously neutron. Again, the fact that gamma-rays with energies up to 4.44 MeV deposit no more than 750 keV$_{ee}$ in the Arktis NDT is striking. This property of the detector greatly facilitates the identification of fast neutrons depositing more energy than this value.

## 6. Summary

A first comparison between the PSD characteristics of a novel $^4$He-based high-pressure gas scintillation detector and a standard NE-213 liquid-scintillator

reference detector has been performed. A Pb-screened Am/Be mixed-field neutron and gamma-ray source was used to irradiate the detectors and a high-resolution scintillation-pulse digitizer was used to optimize the PSD using the tail-to-total method. The NE-213 liquid-scintillator reference cell was differentially very sensitive to the incident gamma-rays and registered a wide range of scintillation-light yields up to 4.4 $MeV_{ee}$. In contrast, the $^4$He-based NDT was designed to have has a low gamma-ray sensitivity. It registered a maximum scintillation-light yield of 750 $keV_{ee}$ for the same distribution of incoming gamma-rays. The PSD obtained with the NE-213 liquid-scintillator reference cell, facilitated by using the digitizer, was good. Clear separation between neutrons and gamma-rays was obtained down to about 0.5 $MeV_{ee}$. The PSD obtained with the $^4$He-based NDT was excellent. Clear separation between neutrons and gamma-rays was obtained down to 0.1 $MeV_{ee}$. Most striking was the fact that gamma-rays of energies up to 4.44 MeV resulted in scintillation-light yields of no more than 750 $keV_{ee}$ in the NDT. As a result, a simple threshold cut above 750 $keV_{ee}$ was sufficient to distinguish fast neutrons from gamma-rays in this region. For fast-neutron detection, $^4$He-based high-pressure gas scintillation detectors such as the NDT thus have a clear advantage over liquid-scintillator detectors such as the NE-213 reference cell when the scintillation-light yield is greater than 750 $keV_{ee}$.

The next step in our investigations shall involve an expanded systematic comparison of the PSD obtained with these two scintillators using a FOM as a function of scintillation-light yield. The scintillation-light yield as a function of neutron energy must also be established if the potential for spectroscopy is to be investigated. In order to perform these investigations, knowledge of the incident neutron energies is required. We have recently successfully tested a technique for performing such irradiations with Be-compound neutron sources [46] which relies on well-understood shielding, coincidence, and time-of-flight measurement techniques to produce a polychromatic energy-tagged neutron beam.

**Acknowledgements**

We thank the Photonuclear Group at the MAX IV Laboratory for providing access to their experimental hall and Am/Be source. We acknowledge the support of the UK Science and Technology Facilities Council (Grant nos. STFC 57071/1 and STFC 50727/1).

**References**

[1] Uses of neutrons in engineering and technology, J. Walker, Phys. Technol. 13 (1982) 239, doi: 10.1088/0305-4624/13/6/I01.

[2] United States Committee on Army Science and Technology for Homeland Defense, Board on Army Science and Technology, Division on Engineering and Physical Sciences, National Research Council, Indications and Warning Technologies, in Science and Technology for Army Homeland Security: Report 1, National Academies Press (2003), ISBN: 9780309087018, http://www.nap.edu/openbook.php?record_id=10655.

[3] International Workshop on Fast Neutron Detectors and Applications (FNDA2006), University of Capetown, South Africa (2006), Proceedings of Science (FNDA2006). http://pos.sissa.it/cgi-bin/reader/conf.cgi?confid=25.

[4] 2nd International Workshop on Fast Neutron Detectors and Applications (FNDA2011), Kibbutz Ein Gedi, Israel (2011), JINST 7 C (2012). http://iopscience.iop.org/1748-0221/focus/extra.proc19.

[5] Proceedings from the workshop on Neutron, Neutrino, Nuclear, Muon and Medical Physics at ESS, Lund, Sweden (2009). http://www.hep.lu.se/staff/christiansen/proceeding.pdf.

[6] Fast neutron detection in homeland security applications, R. Chandra, G. Davatz, U. Gendotti, A. Howard, IEEE NSS/MIC (2010) 508, doi: 10.1109/NSSMIC.2010.5873813.

[7] Drilling and Well Completions, Reservoir Engineering, in Standard Handbook of Petroleum and Natural Gas Engineering, 2nd edition, W.C. Lyons, G.J. Plisga, Elsevier Science (2011), ISBN: 978-0-7506-7785-1.

[8] Fast neutron detection with pressurized $^4$He scintillation detectors, R. Chandra, G. Davatz, H. Friederich, U. Gendotti, D. Murer, JINST 7.03 (2012) C03035, doi: 10.1088/1748-0221/7/03/C03035.

[9] Testing on novel neutron detectors as alternative to $^3$He for security applications, P. Peerani, A. Tomanin, S. Pozzi, J. Dolan, E. Miller, M. Flaska, M. Battaglieri, R. De Vita, L. Ficini, G. Ottonello, G. Ricco, G. Dermody, C. Giles, Nucl. Instr. and Meth. in Phys. Res. A 696 (2012) 110, doi: 10.1016/j.nima.2012.07.025.

[10] Workshop on fast neutron applications at spallation sources, Abingdon, UK (2013). http://plone.esss.lu.se/.

[11] Current Practice in Well Logging, Reservoir Engineering and Secondary Recovery, in The Petroleum Engineering Handbook: Sustainable Operations, M.R. Islam, M.I. Khan, Elsevier Science (2013), ISBN: 9780127999838, http://books.google.com/books?id=xXijAQAAQBAJ.

[12] Analysis for In-situ Fission Rate Measurements using 4He Gas Scintillation Detectors, 3rd International Conference on Advancements in Nuclear Instrumenation Measurement Methods and their Applications, J.L. Lewis, D. Raetz, D. Murer, K.A. Jordan, Marseille, France (2013), doi: 10.1109/ANIMMA.2013.6728031.

[13] Characterization of a cubic EJ-309 liquid scintillator detector, A. Tomanin, J. Paepen, P. Schillebeeckx, R. Wynants, R. Nolte, A. Lavietes, Nucl. Instr. and Meth. in Phys. Res. A 756 (2014) 45, doi: 10.1016/j.nima.2014.03.028.

[14] Fission signal detection using helium-4 gas fast neutron scintillation detectors, J.M. Lewis, R.P. Kelley, D. Murer, K.A. Jordan, Appl. Phys. Lett. 105 (2014) 014102, doi: 10.1063/1.4887366.

[15] Time dependence of liquid-helium fluorescence, D.N. McKinsey, C.R. Brome, S.N. Dzhosyuk, R. Golub, K. Habicht, P.R. Huffman, E. Korobkina, S.K. Lamoreaux, C.E.H. Mattoni, A.K. Thompson, L. Yang, J.M. Doyle, Phys. Rev. A 67 (2003) 062716, doi: 10.1103/PhysRevA.67.062716.

[16] Scintillation detectors, in Noble gas detectors, E. Aprile, A.E. Bolotnikov, A.I. Bolozdynya, T. Doke, Wiley-VCH Verlag GmbH, KGaA, Weinheim Germany (2006), ISBN: 978-3-527-40597-8

[17] The theory and practice of scintillation counting, J.B. Birks, D.W. Fry, L. Costrell, K. Kandish, Pergamon Press, New York, U.S.A. (1964), ISBN: 978-0-08-010472-0.

[18] Radiation detection and measurement, G.F. Knoll, Wiley, New York, U.S.A. (1989), ISBN: 9780471815044, http://books.google.com/books?id=dyBRAAAAMAAJ.

[19] The mechanism of noble gas scintillation, in Elementary particles and cosmic rays, B.A. Dolgosheim, B.U. Rodionov, Volume 2, Atomizdat, Moscow Russia (1969).

[20] NE213 is no longer produced. Eljen Technologies offers EJ-301 (http://www.eljentechnology.com/index.php/products/liquid-scintillators/71-ej-301) while Saint Gobain offers BC-501 (http://www.detectors.saint-gobain.com/uploadedFiles/SGdetectors/Do

[21] supplied by High Tech Sources Limited, Unit 6, Moorbrook, Southmead, Industrial Estate, Didcot, Oxfordshire, UK OX11 7HP; https://www.hightechsource.co.uk.

[22] testing performed at National Physical Laobratory, Teddington, Middlesex, UK TW11 0LW on 24 January 2012.

[23] http://www.hightechsource.co.uk/Legacy/Resources/Americium-Beryllium.pdf for details.

[24] Neutron Spectra of $^{214}$Am/B, $^{241}$Am/Be, $^{241}$Am/F, $^{242}$Cm/Be, $^{238}$Pu/$^{13}$C and $^{252}$Cf isotopic neutron sources, E.A. Lorch, Int. J. Appl. Radiat. Is. 24 (1973) 585, doi: 10.1016/0020-708X(73)90127-0.

[25] The neutron spectrum of Am-Be neutron sources, A.D. Vijaya, A. Kumar, Nucl. Instrum. and Meth. 111 (1973) 435, doi: 10.1016/0029-554X(73)90199-7.

[26] Determination of 4.438 MeV $\gamma$-ray to neutron emission ratio from a $^{241}$Am-$^{9}$Be neutron source, A.A Mowlavi, R. Koohi-Fayegh, Appl. Radiat. Isot. 60 (2004) 959, doi: 10.1016/j.apradiso.2004.02.008.

[27] The 4.438 MeV gamma to neutron ratio for the AmBe neutron source, Zhenzhou Liu, Jinxiang Chen, Pei Zhu, Yongming Li, Guohui Zhang, Appl. Radiat. Isot. 65 (2007) 1318, doi: 10.1016/j.apradiso.2007.04.007.

[28] http://www.laurussystems.com/products/products_pdf/LS_thermo_FH-40.pdf

[29] Polytetrafluoroethylene, also known as Teflon. http://www2.dupont.com/Teflon_Industrial/en_US/products/selection_guides/coatings.html.

[30] D.N. McKinsey, C.R. Bromea, J.S. Butterworth, S.N. Dzhosyuk, R. Golub, K. Habicht, P.R. Huffman, C.E.H. Mattoni, L. Yang, J.M. Doyle Detecting ionizing radiation in liquid helium using wavelength shifting light collection, Nuc. Instr. Meth. 516, Issue 2-3, p. 475-485.

[31] http://www.hamamatsu.com/us/en/R580.html

[32] http://www.eljentechnology.com/index.php/products/paints/87-ej-520.

[33] http://www.us.schott.com/borofloat/english/index.html for details. Supplied by Glasteknik i Emmaboda AB, Utvägen 6 SE-361 31 Emmaboda, Sweden.

[34] Araldite is a registered trademark of Huntsman. See http://www.araldite2000plus.com.

[35] Viton is a registered trademark of DuPont Performance Elastomers LLC.

[36] Poly(methyl-methacrylate), also known as acrylic, plexiglass, and lucite. Supplied by Nordic Plastics Group AB, Bronsyxegatan 6, SE-213 75 Malmö, Sweden.

[37] http://www.eljentechnology.com/index.php/products/pmma-a-uvt-material/102-light-guides

[38] http://www.eljentechnology.com/index.php/products/paints/86-ej-510.

[39] http://www.et-enterprises.com/files/file/Pmtbrochure11.pdf for details.

[40] Arktis Radiation Detectors Limited, 8045 Zürich, Switzerland; http://www.arktis-detectors.com.

[41] S. Ritt, Design and Performance of the 6 GHz Waveform Digitizing Chip DRS4, in IEEE Nuclear Science Symposium Conference, NSS 08, Oct 2008, pp. 1512-1515.

[42] A Scalable DAQ System Based on the DRS4 Waveform Digitizing Chip, H. Friederich, G. Davatz, U. Hartmann, A. Howard, H. Meyer, D. Murer, S. Ritt, N. Schlumpf, IEEE Trans. Nucl. Sci. 58 (2011) 1652, doi: 10.1109/TNS.2011.2159623.

[43] A technique for determining bias settings for organic scintillators, H.H. Knox, T.G. Miller, Nucl. Instrum. and Meth. 101 (1972) 519, doi: 10.1016/0029-554X(72)90040-7.

[44] S. Agostinelli et al., Geant 4: A Simulation toolkit, Nucl. Instrum. Meth. A 506 (2003) 250, doi: 10.1016/S0168-9002(03)01368-8.

[45] J. Allison et al., Geant4 developments and applications, IEEE Trans. Nucl. Sci. 53 (2006) 270, doi: 10.1109/TNS.2006.869826.

[46] Tagging fast neutrons from an $^{241}$Am/$^{9}$Be source, J. Scherzinger, J.R.M. Annand, G. Davatz, K.G. Fissum, U. Gendotti, R. Hall-Wilton,

E. Håkansson, R. Jebali, K. Kanaki, M. Lundin, B. Nilsson, A. Rosborg, H. Svensson, Applied Radiation and Isotopes 98 (2015) 74, doi: 10.1016/j.apradiso.2015.01.003.